Catal Lett (2008) 124:1–6
DOI 10.1007/s10562-008-9530-5

Methane Partial Oxidation Using A $(La_{0.6}Sr_{0.4})(Ga_{0.8}Mg_{0.05}Co_{0.15})O_{3-\delta}$ Membrane

Yuanbo Lin · Manoj R. Pillai · David M. Bierschenk · Blake L. Stevens · Scott A. Barnett

Received: 4 April 2008 / Accepted: 29 May 2008 / Published online: 17 June 2008

Abstract This article describes results on methane partial oxidation in $(La_{0.6}Sr_{0.4})(Ga_{0.8}Mg_{0.05}Co_{0.15})O_3$ ceramic membrane reactors. The thin membranes were fabricated by co-firing with porous composite NiO–La-doped Ceria (LDC) supports. A $La_{0.6}Sr_{0.4}Fe_{0.2}Co_{0.8}O_3$-based composite layer on the air side of the membrane promoted fast oxygen reduction. Electrical measurements indicated that LSGMC showed good mixed conductivity and that oxygen transport was co-limited by bulk and interfacial processes. The O_2 permeation rate during methane partial oxidation at 750 °C was $\approx$10–12 sccm/cm^2, with a maximum syngas production rate of 60–70 sccm/cm^2.

Keywords Mixed conductor · Membrane · Methane · Partial oxidation · Lanthanum Gallate · Ni

1 Introduction

Ceramic membranes that exhibit both electronic and oxygen ion conductivity have a number of applications [1–3], including separation of pure oxygen from air [4–6], providing pure oxygen for partial oxidation of hydrocarbons [1, 4, 7–9], and producing pure hydrogen (via extraction of oxygen from H_2O) [10]. Much of the research has focused on acceptor-doped perovskite oxides [11, 12]. Table 1 summarizes the performance of some of the key materials that have been tested as oxygen permeation membranes for partial oxidation reactors [7, 9, 12–20]. While many of these materials provide high oxygen fluxes of $\sim$10 sccm cm^{-2} at 850–900 °C, some are unstable in the highly-reducing gases encountered in methane partial oxidation [21]. Good stability has been achieved by maintaining $LaFeO_3$-based membranes under operating conditions that are moderately reducing [22]. Stability can also be improved by co-doping the material with less reducible ions, e.g., Zr^{4+} and Ga^{3+}. The gallate materials, such as $(La,Sr)(Ga,Fe)O_3$ [8, 23–26], appear to be especially promising regarding their stability.

The above membranes have been studied primarily in bulk form, requiring relatively high temperatures to achieve high oxygen permeation rates. In addition, in the case of thick gallate membranes, the high cost of Ga may be prohibitive. Thus, thin supported gallate-based membranes could be useful to provide high oxygen flux at relatively low membrane temperatures and at reasonable materials cost. Little work has been done to date on thin mixed-conducting gallate-based membranes.

In this article, we describe initial results on thin $(La_{0.6}Sr_{0.4})(Ga_{0.8}Mg_{0.05}Co_{0.15})O_3$ (LSGMC) membranes and their application for methane partial oxidation [27]. This composition is similar to the ionically conducting composition $(La_{0.6}Sr_{0.4})(Ga_{0.8}Mg_{0.2})O_3$ (LSGM), that has been widely used in thin-electrolyte solid oxide fuel cells. Co doping introduces substantial electronic conductivity while increasing the ionic conductivity, thereby making it a candidate membrane material. The 15% Co composition

Y. Lin · M. R. Pillai · D. M. Bierschenk · B. L. Stevens · S. A. Barnett (✉)
Department of Materials Science and Engineering, Northwestern University, Evanston, IL 60208, USA
e-mail: s-barnett@northwestern.edu

Present Address:
Y. Lin
Diamond Innovations, 6325 Huntley Road, Worthington, OH 43035, USA

Present Address:
M. R. Pillai
Functional Coating Technology, Evanston, IL 60201, USA

Table 1 Reported oxygen permeation rate values for syngas generation experiments

Membrane material	O_2 permeation (sccm/cm^2)	Temperature (°C)	Reference
$SrFeCo_{0.5}O_x$	2–4	850	[17, 18]
$SrFeCo_{0.5}O_x$	3	900	[7, 13]
$SrCo_{0.8}Fe_{0.2}O_3$	3	875	[12]
$Ba_{0.5}Sr_{0.5}Co_{0.8}Fe_{0.2}O_3$	11.5	875	[19]
$BaCo_{0.4}Fe_{0.4}Zr_{0.2}O_3$	5.6	850	[14]
$La_{0.2}Sr_{0.8}Co_{0.8}Fe_{0.2}O_3$	0.8	900	[9]
$La_{0.8}Sr_{0.2}Co_{0.1}Fe_{0.8}Cr_{0.1}O_3$	14.5	900	[39]
$La_{0.3}Sr_{1.7}Ga_{0.6}Fe_{1.4}O_{5+\delta}$	6–7	900	[16]
$Pr_2(Ni_{0.75}Cu_{0.2}Fe_{0.05})O_4$	1.5–5.5	800–1000	[15]

was chosen for the present study because the ionic conductivity peaks at ≈0.15 S/cm at 800 °C near this composition, and the ionic transport number t_i is reasonably low, 0.7 (measured at 1000 °C) [28]. The membrane structures consisted of a porous Ni-LDC support, a dense LDC layer, a dense LSGMC layer, and a porous layer that consisted of 50 wt% $La_{0.6}Sr_{0.4}Fe_{0.2}Co_{0.8}O_3$ (LSCF) and 50 wt% LSGM. The Ni–La-doped Ceria (Ni-LDC) and LSCF-LSGM layers had high surface area to promote fast oxygen transport across membrane interfaces at moderate temperatures; they have similarly been used as an intermediate-temperature SOFC anode [29] and cathode [30], respectively. The Ni-LDC served not only as a support and a surface layer, but also as a reforming catalyst for partial oxidation. It has been shown that such Ni-based supports can be coke-free in direct-methane SOFCs when a substantial oxygen flux is maintained [31, 32]. The LDC barrier layer and Ni-LDC support compositions were chosen to avoid out-diffusion of La from the LSGM electrolyte and Ni-LSGM reactions during high-temperature co-firing of the membrane structure; a similar strategy has been successfully used in LSGM-electrolyte SOFCs [33]. Note that the LDC layer is on the reducing side of the catalytic membrane, where it exhibits mixed conductivity [29].

2 Experimental Procedures

$(La_{0.6}Sr_{0.4})(Ga_{0.8}Mg_{0.05}Co_{0.15})O_3$ (LSGMC) powder was prepared by solid-state reaction. La_2O_3, $SrCO_3$, Ga_2O_3, CoO, and MgO, in amounts indicated by the above LSGMC composition, were mixed in ethanol for 24 h. The slurry was dried and fired at 1250 °C for 12 h. The $(La_{0.6}Sr_{0.4})(Ga_{0.8}Mg_{0.2})O_3$ (LSGM) powder used in the air-side catalytic layer was prepared in a similar fashion. $La_{0.4}Ce_{0.6}O_{2-\delta}$ (LDC) powder was also produced by solid-state reaction of La_2O_3 and CeO_2 after firing at 1250 °C for 12 h. After grinding and sieving with 200# mesh, the powders were studied with X-ray diffraction (XRD) in a diffractometer with Cu K_α radiation. The XRD patterns were analyzed and determined with Jade 6.5 software. The results showed good agreement with expected peaks for LSGMC, LSGM, and LDC [8], with no indication of secondary phases. Commercial LSCF powder (Praxair) was used in the air-side catalytic layer, and commercial NiO (Alfa Aesar) in the fuel-side catalytic layer.

The Ni-LDC supports were prepared as follows. Commercial NiO (Alfa Aesar) and the above-described LDC powder with weight ratio 3:2 were ball milled together for 24 h in ethanol with 10 wt% starch as a pore former and 0.5 wt% polyvinyl butyral (PVB) as a binder. The milled powder mixture was dried and pressed into pellets with a diameter of 19 mm and a thickness of ≈0.6 mm. The pellets were bisque fired at 1100 °C for 4 h. LDC and LSGMC colloidal suspensions were prepared by mixing the powder with a binder and dispersant in ethanol. Layers of LDC and LSGMC were fabricated by sequentially drop coating the LDC and LSGMC colloidal solutions on the Ni-LDC supports. The resulting assembly was co-sintered at 1400 °C for 4 h. The final thicknesses of LDC (5 μm) and LSGM (8–10 μm) were controlled by the amount of colloidal solution applied onto the support. The LSCF-LSGM layer was deposited by screen printing, using an ink prepared by mixing the powders with a commercial vehicle (Heraeus V737) in a three-roll mill, followed by firing at 1100 °C for 1 h.

The Ni-LDC side of each membrane structure was sealed to an alumina support tube using Ag ink (DAD-87, Shanghai Research Institute of Synthetic Resin). The membranes were placed inside a furnace that maintained the temperature from 550 to 750 °C. Either hydrogen or methane was supplied through an alumina feed tube mounted concentrically within the alumina support tube. Stagnant air was present at the LSCF-LSGM side of the membrane. At the beginning of testing the membranes were heated to 600 °C and maintained at this temperature for 12 h in humidified hydrogen, which reduced the NiO-LDC supports to Ni-LDC. A gas

chromatograph was used to measure the membrane product gases, except for H_2O which was removed by a desiccant, while flowing dry methane at rates of 10–50 sccm.

Although this structure was designed as a partial oxidation membrane, the conducting Ni-LDC and LSCF-LSGM layers allowed electrical characterization. Thus, Ag-wire contacts were connected to the electrodes using Ag ink. Open-circuit voltage and current-voltage curves were measured using an Electrochemical Workstation (IM6, ZAHNER), with the cathode exposed to ambient air and the anode to humidified (3% H_2O) hydrogen at a flow rate of 100 sccm. The frequency range for the impedance measurement was 0.1 Hz to 1 MHz. The cell structure was observed after testing using scanning electron microscopy (SEM) in a Hitachi S-3400 N-II microscope.

3 Results and Discussion

Figure 1 shows a fracture cross-sectional SEM image and EDS chemical maps of a typical membrane structure after partial oxidation measurements. The elements detected were all contained within the expected layers and well-defined interfaces were observed. There was no evidence of any reaction between Ni and LSGMC or loss of La from the LSGMC. Furthermore, the image appeared to be identical to images taken prior to measurements, indicating that there was no structural degradation of the membrane during partial oxidation. The LSGMC/LDC membrane appeared to be quite dense; membrane gas tightness was verified by gas chromatography (GC) measurements that showed <1% N_2 in the gas stream for typical methane flow rates. The Ni-LDC support showed pores with a size scale of $\sim$1 μm, whereas the LSCF-LSGM layer showed $\sim$0.3 μm pores. Larger pores were present in the Ni-LDC support further from the LSGMC/LDC membrane (outside of the view of this SEM image) due to the pore former that had been added to the powders.

Membrane reactor products were measured using gas chromatography. To ensure that the test system did not contribute to methane reforming, a blank reactor was first tested. The blank reactor, when tested with air-methane mixtures, showed minimal hydrogen and carbon monoxide generation as measured by GC. Figure 2 shows the reaction products from a typical membrane operated at 750 °C, versus methane flow rate. As the flow rate decreased, the methane content decreased and the H_2, CO_2, and CO contents increased. This is expected assuming that the oxygen flux through the membrane remained constant, such that the O_2-to-CH_4 ratio increased as the CH_4 flow decreased. Methane conversion to H_2 and CO should reach a maximum near an O_2/CH_4 ratio of 0.5, i.e., the stoichiometry of partial oxidation ($CH_4 + (1/2)O_2 = H_2 + CO$). Since the CO and H_2

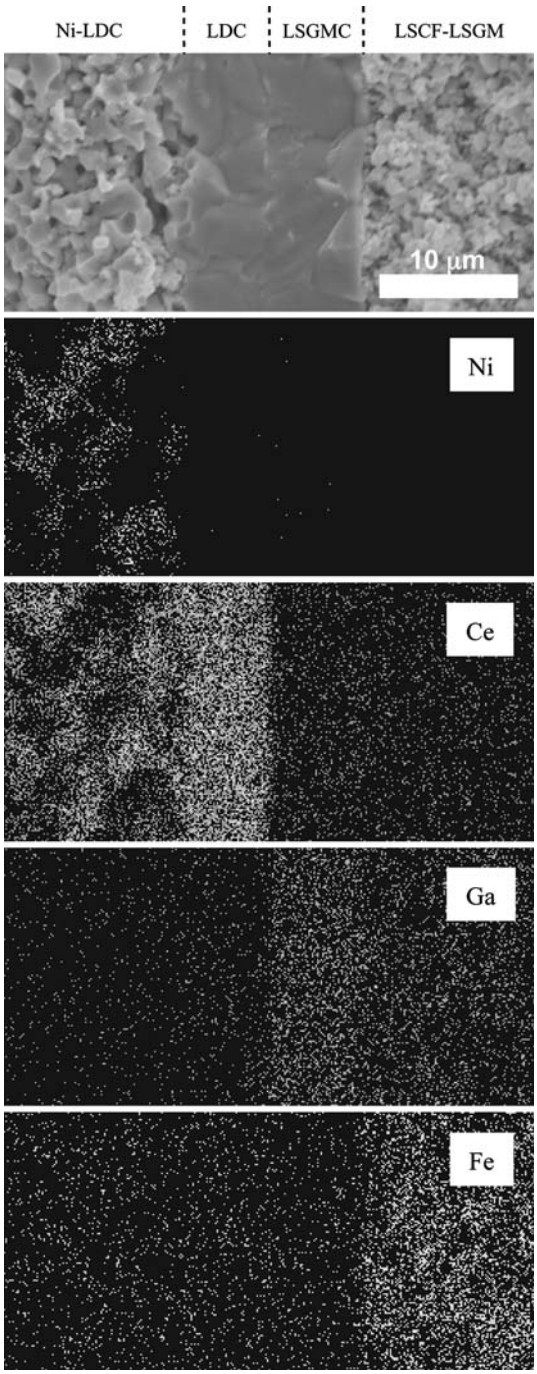

Fig. 1 Fracture cross sectional SEM image and EDS element maps of a membrane structure after partial oxidation measurements

contents reached maxima at a methane flow rate of $\approx$10–15 sccm, this suggests that the oxygen flux through the membrane corresponded to $\sim$5–7.5 sccm O_2 at 750 °C. Given that the active area of the membrane was 0.5 cm^2, the flux per unit area was $\sim$10–15 sccm O_2/cm^2. A more accurate estimate of the oxygen flux was obtained for each gas composition from the amount of oxygen in the products. For this calculation, we assumed that the steam content was twice the CO_2

content, a ratio expected because of the 2:1 ratio of H_2 to C in methane. The calculated oxygen flux ranged from 11 to 13 sccm O_2/cm^2. This oxygen flux is comparable to the best membranes shown in Table 1, despite the fact that the current membranes were operated at a temperature 100–150 °C lower. A few experiments carried out at a higher temperature of 800 °C showed an ≈50% higher membrane oxygen flux.

The measured CH_4 and CO_2 mole fractions were higher and the H_2 and CO fractions lower in Fig. 2 than the thermodynamic equilibrium predicted gas compositions at 750 °C. For O_2/CH_4 = 0.5, for example, the equilibrium mole fractions are 4 % CH_4, 2% CO_2, 60% H_2, 30% CO, and 4% H_2O. This may indicate that the membrane produces H_2O and CO_2 as initial products, but that these incompletely reform the CH_4 to H_2 and CO in the Ni-LDC support. Similar results and explanations have been reported for electrochemical partial oxidation of methane in solid oxide fuel cells [34].

The data in Fig. 2 were taken during the first several hours of membrane operation. Figure 3 shows the exhaust gas composition versus time for a typical test. The flow rate was decreased from 15 to 10 sccm after 8 h, resulting in an increase in methane conversion in agreement with the results in Fig. 2. The amounts of H_2 and CO decreased continuously (aside from the change in flow rate), whereas the methane and CO_2 increased. Analysis of the results showed that the amount of oxygen in the products did not change, indicating that the membrane oxygen transport was not degrading. Rather, the decreased methane conversion appeared due to reduced catalytic activity in the Ni-LDC layer. This decreased activity was not due to coking [35, 36], as EDS observations showed no evidence of any carbon on the Ni-LDC after degradation. The lack of coking has

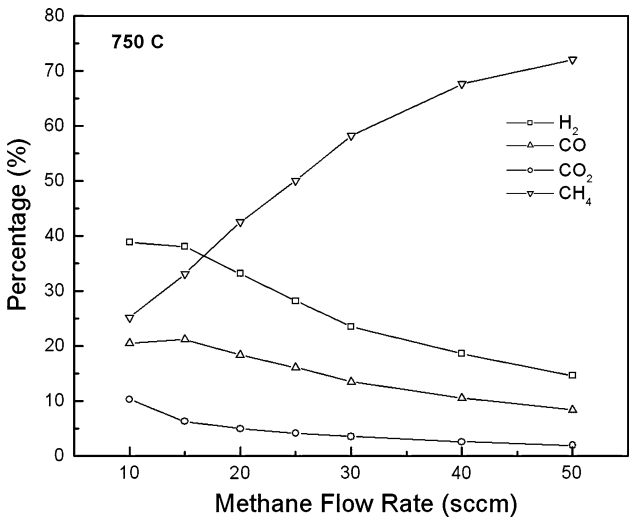

Fig. 2 Reaction product composition versus methane flow rate in the LSGMC membrane reactor at 750 °C

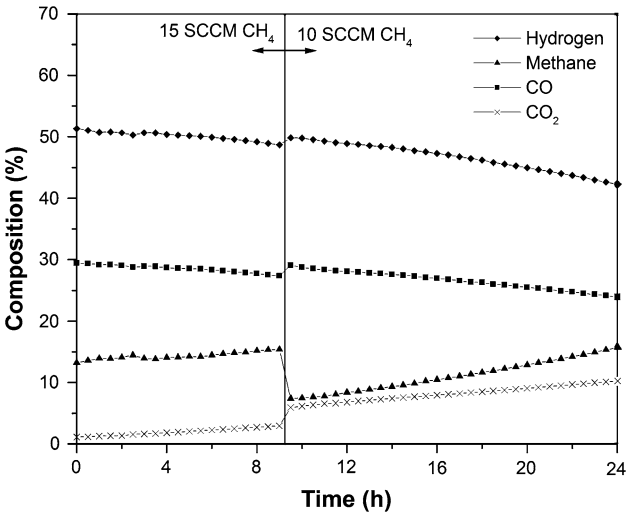

Fig. 3 Exhaust gas composition versus time of a membrane operated at 750 °C. The initial methane flow rate of 15 sccm was reduced to 10 sccm part way through the test

previously been explained in direct-methane SOFCs with Ni-based anodes by the presence of large concentrations of H_2O and CO_2 products in the exhaust for high oxygen ion fluxes [32]. On the other hand, the decrease in reforming activity is similar to that observed previously in Ni-YSZ SOFC anodes. [34, 37, 38] These anodes, like the present Ni-LDC supports, were fired at a high temperature of ∼1400 °C, and hence they exhibited micron-scale Ni particles with relatively low surface area and low reforming activity. However, a small amount of Ni dissolved in the oxide phase during firing, and then precipitated out upon exposure to a reducing environment, resulting in the nucleation of Ni nano-particles that were visible in TEM images. These particles have a high surface area but coarsen over time, yielding a high initial reforming activity that gradually degrades.

Figure 4 shows the electrical characteristics of a typical structure at temperatures ranging from 550 to 750 °C, with air at the LSCF-LSGM side and humidified hydrogen (30 sccm) at the Ni-LDC side. The measured open circuit voltage V_{OC} decreased from 0.68 at 550 °C to 0.66 at 750 °C. For comparison, the calculated Nernst potential E_N for air and humidified hydrogen varied from 1.14 V at 550 °C to 1.11 V at 750 °C. The ionic transport number can be estimated from the expression [39]

$$t_i = V_{OC}/E_N,$$

which yields $t_i \approx 0.59$ at 750 and 550 °C. Accounting for the effect of electrode polarization will result in an upwards correction of t_i, [40] such that the present value is consistent with the value t_i = 0.7 reported for this LSGMC composition at 1000 °C [28].

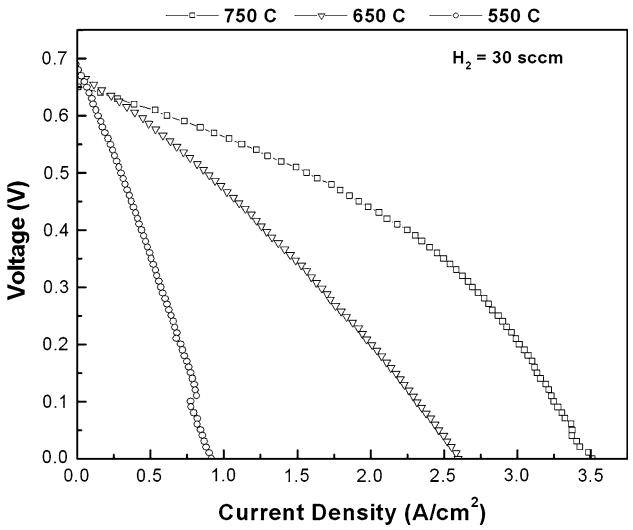

Fig. 4 Current–voltage characteristics obtained at different temperatures from an LSGMC membrane structure operated with hydrogen on the Ni-LDC side and air on the LSCF-LSGM side of the membrane

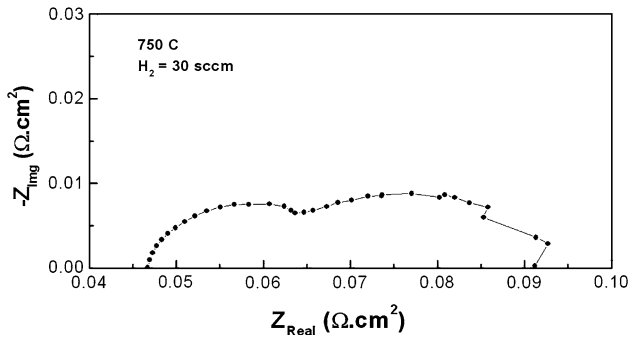

Fig. 5 Typical EIS spectrum from a membrane operated at 750 °C

Electrochemical impedance spectroscopy measurements on the membrane at 750 °C are shown in Fig. 5. These provide insight into the processes that limit oxygen transport through the membrane. The high-frequency intercept of the impedance arc with the real axis corresponds to the ohmic loss, mainly associated with combined oxygen and electron transport across the LSGMC/LDC membrane. The total width of the impedance arc corresponds to the interfacial mechanisms occurring at the membrane surface layers, i.e., mass transport and charge exchange. It is apparent that both interfacial and volume processes significantly limit membrane performance.

4 Conclusions

The present results show that LSGMC membranes provide a relatively high oxygen flux for methane partial oxidation at a relatively low temperature of 750 °C. The Ni-based membrane support did not coke during operation in methane at 750 °C, but did not provide sufficient reforming activity to fully convert the methane to syngas. This could be remedied by using a higher temperature (which would also increase the oxygen flux), a more active catalyst composition or morphology, or by using an additional down-stream catalyst.

Acknowledgments This material is based upon work supported by the MRSEC program of the National Science Foundation (DMR-0520513) at the Materials Research Center of Northwestern University and by the Department of Energy Solid State Conversion Alliance (SECA) Program, obtained via a subcontract from Ceramatec Inc.

References

1. Bouwmeester HJM (2003) Catal Today 82:141
2. Julbe A, Farrusseng D, Guizard C (2005) Catal Today 104:102
3. Sundmacher K, Rihko-Struckmann LK, Galvita V (2005) Catal Today 104:185
4. Dyer PN, Richards RE, Russek SL, Taylor DM (2000) Solid State Ionics 134:21
5. Ito W, Nagai T, Sakon T (2007) Solid State Ionics 178:809
6. Kharton VV, Yaremchenko AA, Kovalevsky AV, Viskup AP, Naumovich EN, Kerko PF (1999) J Membr Sci 163:307
7. Balachandran U, Dusek JT, Maiya PS, Ma B, Mieville RL, Kleefisch MS, Udovich CA (1997) Catal Today 36:265
8. Ishihara T, Tsuruta Y, Todaka T, Nishiguchi H, Takita Y (2002) Solid State Ionics 152–153:709
9. Tong J, Yang W, Cai R, Zhu B, Lin L (2002) Catal Lett 78:129
10. Balachandran U, Lee TH, Wang S, Dorris SE (2004) Int J Hydrogen Energy 29:291
11. Teraoka Y, Nobunaga T, Yamazoe N (1988) Chem Lett 17:503
12. Teraoka Y, Zhang HM, Furukawa S, Yamazoe N (1985) Chem Lett 14:1743
13. Balachandran U, Dusek JT, Mieville RL, Poeppel RB, Kleefisch MS, Pei S, Kobylinski TP, Udovich CA, Bose AC (1995) Appl Catal A 133:19
14. Balachandran U, Dusek JT, Sweeney SM, Poebbel RB, Mieville RL, Mayia PS, Kleefish MS, Pei S, Kobylinski TP, Udovich CA, Bose A (1995) Am Ceram Soc Bull 74:71
15. Ishihara T, Miyoshi S, Furuno T, Sanguanruang O, Matsumoto H (2006) Solid State Ionics 177:3087
16. Schwartz M, White JH, Sammels AF (2000) US Patent 6,033,632
17. Shao Z, Dong H, Xiong G, Cong Y, Yang W (2001) J Membr Sci 183:181
18. Shao Z, Xiong G, Dong H, Yang W, Lin L (2001) Sep Purif Technol 25:97
19. Tsai C-Y, Dixon AG, Ma YH, Moser WR, Pascucci MR (1998) J Am Ceram Soc 81:1437
20. Stevenson JW, Armstrong TR, Pederson LR, Weber WJ (1995) Proceedings of the first international symposium on ceramic membranes, Chicago, IL
21. Pei S, Kleefisch MS, Kobylinski TP, Faber J, Udovich CA, Zhang-McCoy V, Dabrowski B, Balachandran U, Mieville RL, Poeppel RB (1994) Catal Lett 30:201
22. Carolan M (2006) Presentation to the Chicago Catalysis Club, Des Plaines, IL, February
23. Etchegoyen G, Chartier T, Julian A, Del-Gallo P (2006) J Membr Sci 268:86

24. Kharton VV, Shaulo AL, Viskup AP, Avdeev M, Yaremchenko AA, Patrakeev MV, Kurbakov AI, Naumovich EN, Marques FMB (2002) Solid State Ionics 150:229
25. Shaula AL, Kharton VV, Marques FMB (2004) J Eur Ceram Soc 24:2631
26. Shaula AL, Viskup AP, Kharton VV, Logvinovich DI, Naumovich EN, Frade JR, Marques FMB (2003) Mater Res Bull 38:353
27. Ishihara T, Tabuchi J, Ishikawa S, Yan J, Enoki M, Matsumoto H (2006) Solid State Ionics 177:1949
28. Ishihara T (2003) In: Vielstich W, Lamm A, Gasteiger HA (eds) Handbook of fuel cells—fundamentals, technology and applications, vol. 4: fuel cell technology and applications. John Wiley & Sons Ltd., Hoboken, NJ
29. Huang K, Wan J-H, Goodenough JB (2001) J Electrochem Soc 148:A788
30. Lin Y, Barnett SA (2008) Solid State Ionics 179:420
31. Lin Y, Zhan Z, Barnett SA (2006) J Power Sources 158:1313
32. Lin Y, Zhan Z, Liu J, Barnett SA (2005) Solid State Ionics 176:1827
33. Lin Y, Barnett SA (2006) Electrochem Solid-State Lett 9:A285
34. Zhan Z, Lin Y, Pillai M, Kim I, Barnett SA (2006) J Power Sources 161:460
35. Takeguchi T, Kani Y, Yano T, Kikuchi R, Eguchi K, Tsujimoto K, Uchida Y, Ueno A, Omoshiki K, Aizawa M (2002) J Power Sources 112:588
36. Baker RTK, Harris PS, Henderson J, Thomas RB (1975) Carbon 13:17
37. King DL, Strohm JJ, Wang X, Recknagle KP, Singh P, Wang Y (2006) DoE SECA Review Meeting, Philadelphia
38. Pillai MR, Bierschenk DM, Barnett SA (2008) Catal Lett 121:19
39. Wagner C (1933) Z Phys Chem B Chem Elem Proz Aufbau Mater 21:25
40. Matsui T, Kosaka T, Inaba M, Mineshige A, Ogumi Z (2005) Solid State Ionics 176:663